Submitted, accepted and published by:
Energy Conversion and Management 159 (2018) 221-231

Chemical Looping Combustion of gaseous and solid fuels with manganese-iron mixed oxide as oxygen carrier

Raúl Pérez-Vega, Alberto Abad*, Francisco García-Labiano, Pilar Gayán, Luis F. de Diego, María Teresa Izquierdo, Juan Adánez

Instituto de Carboquímica (ICB-CSIC), Dept. of Energy & Environment, Miguel Luesma Castán 4, 50018-Zaragoza, Spain.

* Corresponding author: A. Abad.

E-mail address: abad@icb.csic.es; phone: +34 976 733 977; fax: +34 976 733 318.

Abstract

Synthetic manganese-iron mixed oxides are considered promising materials to be used as oxygen carriers for Chemical Looping Combustion of coal with carbon dioxide capture at low cost. The aim of this work was to evaluate a manganese-iron mixed oxide material with a manganese to iron molar ratio of 0.77:0.23 as oxygen carrier for coal combustion by means of chemical looping processes, including both *ex-situ* and *in-situ* gasification of coal. The preparation method -spray drying followed by calcination- was optimized in order to produce particles with high reactivity and mechanical strength. The material was studied in two continuously operated facilities designed to burn either gaseous or solid fuels. While full combustion was achieved burning syngas, showing the feasibility of the use of this material considering the *ex-situ* gasification process. Coal combustion efficiency by *in-situ* gasification process was improved in comparison with other previously tested low-cost materials such as ilmenite and iron ore. Moreover, the oxygen carrier particles showed an interesting magnetic behavior that was able to facilitate oxygen carrier recovery from the

purge ash stream. In view of these results, the manganese-iron mixed oxide as oxygen carrier is proposed as a promising candidate for use coal combustion by the chemical looping process.

Keywords: CO_2 capture; Chemical Looping Combustion; Oxygen carriers; Manganese-Iron mixed oxide; Coal.

1. Introduction

Nearly 70 % of global carbon dioxide (CO_2) emissions are the result of the use of fossil fuels in power generation, of which coal is the most carbon-intensive fossil fuel [1]. This figure highlights the need for clean coal combustion technologies, such as those allowing CO_2 capture, in order to minimize CO_2 emissions. Several emerging CO_2 capture technologies including chemical looping processes, adsorption systems based on solid sorbents [2], and membrane separation systems [3] have been tagged as the most promising CO_2 capture modes. A review of all these technologies and their advantages and disadvantages can be consulted elsewhere [4]. Of these, Chemical Looping Combustion (CLC) has as main advantage of CO_2 capture being inherent to the process, which considerably reduces the cost per the tonne of CO_2 captured [5].

1.1. Chemical looping concepts for coal combustion

The CLC concept is based on the transfer of oxygen from the air to the fuel through an oxygen carrier in order to prevent contact between the air and fuel. Metal oxides are generally used as oxygen carriers because they are easily able to provide the required

oxygen transfer because of their redox properties. Oxygen transfer is achieved by continuously circulating the oxygen carrier between two interconnected fluidized bed reactors: the fuel and air reactors. In the fuel reactor, the fuel is mainly oxidized to carbon dioxide (CO_2) and steam (H_2O) by the reduction of the metal oxide. The reduced oxygen carrier is subsequently transported to the air reactor where it is reoxidized with the oxygen from air. Combustion of coal and other solid fuels (e.g. petcoke or biomass) using CLC technology can be achieved by means of three processes: via *ex-situ* Gasification Chemical Looping Combustion (*e*G-CLC), *in-situ* Gasification Chemical Combustion (*i*G-CLC) and Chemical Looping Oxygen Uncoupling (CLOU) [5].

1.1.1. Chemical looping combustion of coal via *ex-situ* gasification

The *e*G-CLC process involves coal gasification with oxygen in a gasifier to produce syngas, which is subsequently fed into the fuel reactor in the CLC system [6]. High-efficiency power generation is expected by combining CLC with an Integrated Gasification Combined Cycle (IGCC) [7], which requires the use of a pressurized CLC unit, or of Combining Cooling, Heating and Power production (CCHP) [8]. An additional advantage of the *e*G-CLC process is that oxygen carrier particles do not come into contact with the ash from coal, eliminating any possible ash-oxygen carrier interaction or oxygen carrier losses in the ash purge stream. However, the requirement of an external gasifier and oxygen for the coal gasification is an added cost of the process.

Different oxygen carriers have been evaluated by burning syngas with different results. High syngas conversions to CO_2 and H_2O have always been achieved with synthetic materials formed using nickel (Ni), manganese (Mn), iron (Fe) or copper (Cu) oxides as

active phases and supported on inert materials. Johansson et al. [9] achieved combustion efficiencies higher than 99 % through the use of an oxygen carrier with a 40 wt% nickel oxide (NiO) active phase supported on magnesium aluminate ($MgAl_2O_4$). Similar results were obtained by Dueso et al. [10] with another Ni-based material obtained by impregnation of an 18 wt% NiO on alumina. Complete combustion of syngas was obtained by Abad et al. [11] in a 0.3 kW_{th} CLC rig by using a Mn-based oxygen carrier supported on magnesia-stabilized zirconia. Likewise, these authors [12] reached high syngas conversion (99 %) in the same facility with another material by supporting a 60 wt% hematite (Fe_2O_3) on alumina. Forero et al. [13] obtained complete syngas combustion with an oxygen carrier prepared by impregnation of a 14 wt% copper oxide (CuO) on alumina. However, lower combustion efficiencies were achieved by using natural ores as oxygen carriers. Kolbitsch et al. [14] conduced syngas combustion tests with ilmenite ($FeTiO_3$) in a 120 kW_{th} facility. They observed high H_2 oxidation (around 90-95 %) and low carbon monoxide (CO) conversion (around 65-70 %) at fuel input capacities of between 60 and 80 kW_{th}. Syngas conversions of around 85 % were found by Zheng et al. [15] when calcium sulfate ($CaSO_4$) was used as the oxygen carrier.

When selecting an oxygen carrier for CLC using coal gas as fuel the most important aspect to consider is the ability to convert the gaseous fuel to CO_2 and H_2O. In this sense, after a theoretical thermodynamic analysis, Jerndal et al. [16] proposed Cu-, Fe-, and Mn-based materials as the more suitable oxygen carriers. However, other factors, such as cost, sulfur, and environmental aspects should be always taken into account. From an economic perspective, the comprehensive study by Abad et al. [17] on CLC rig operating conditions indicated that the use of an Fe-based oxygen carrier was more advantageous than of Cu- or

Ni-based materials for burning syngas. With regard to sulfur deposition on the oxygen carrier, García-Labiano et al. [18] advised against using Ni-based materials. In this sense, de Diego et al. [19] showed that Fe-based oxygen carriers were sulfur resistant, while the Cu-based materials were sulfur sensitive. Finally, Mendiara et al. [20] analyzed the toxicity of Fe-based materials after their use in a CLC facility, confirming the environmental suitability of the use of these types of materials.

1.1.2. Chemical looping combustion of coal via *in-situ* gasification

In *i*G-CLC, solid fuels are gasified in the fuel reactor using steam and/or recycled CO_2 as gasifying agents. Oxidation of the gasification products to CO_2 and H_2O subsequently takes place by means of a gas-solid reaction with the oxygen carrier. Oxygen carrier losses are expected during ash purging, so the use of low-cost materials is encouraged in order to reduce the cost associated with compensating for those losses. Thus, minerals and wastes materials based on iron and manganese oxides have mostly been evaluated as oxygen carriers for *i*G-CLC where coal or biomass are considered for use as fuels [21]. Gasification is the limiting step for coal conversion, and some unburned char particles may reach the air reactor together the oxygen carrier, which would mean a decrease in CO_2 capture efficiency. A strategy to prevent char particles from reaching the air reactor could consist of raising the residence time of these type of particles inside the fuel reactor. Su et al. [22] observed that this could be achieved through a reduction in the gas velocity at the bottom part of the fuel reactor. However, this action would entail a decrease in the solids circulation rate between the air and fuel reactors [23], which would affect the amount of oxygen available in the fuel reactor. Another alternative for preventing char particles from

reaching the air reactor is to include a carbon stripper between the fuel and air reactors. Pérez-Vega et al. [24] proved that the increase separation efficiency produced by this device, high CO_2 capture efficiency could be achieved without affecting the solids circulation rate. However, complete conversion of the gases to CO_2 and H_2O is not achieved, and unburned products (CO, H_2 and CH_4) appear in the CO_2 stream from *i*G-CLC units [21]. The common option taken to address the presence of unburned products in the CO_2 stream is an oxygen polishing step, which uses pure oxygen to complete the combustion of gases, with the consequent additional cost. Several options have been proposed in order to increase the combustion efficiency of the process, including the use of oxygen carriers with high reactivity [25] or oxygen uncoupling capability [26], and the implementation of technological solutions such as the recirculation of unburned gases or the use of a secondary fuel reactor [27].

1.1.3. Chemical looping combustion of coal via oxygen uncoupling

The CLOU process is based on the use of metal oxides that are capable of generating gas-phase oxygen at high temperature [26]. This allows oxygen to be released inside the fuel reactor and to reacts directly with the coal, increasing the coal conversion rate compared to *i*G-CLC. Coal combustion by CLOU shows improved performance when compared to *i*G-CLC, achieving full combustion, achieving CO_2 capture efficiencies close to 100 % [28]. Similar differences in performance between both types of chemical looping modes were found when biomass was burned [29]. Traditionally, Cu- or Mn-monometallic oxides supported on an inert material have been proposed for their use in CLOU [30]. In addition,

bimetallic systems have recently been considered through the combination of oxides such as Cu-,, Mn-, or Fe-based material [31].

Oxygen carriers consisting of CuO supported on different inert materials have been more commonly evaluated owing to their high oxygen uncoupling capability and the fast kinetics of their decomposition and regeneration reactions [32]. Gayán et al. [33] developed a screening process for Cu-based materials in which they identified two oxygen carriers comprising 40 % CuO on silica and 60 % CuO on $MgAl_2O_4$, respectively as the most suitable combinations. The CuO-based oxygen carrier supported on $MgAl_2O_4$ was used to demonstrate proof of concept of the CLOU process with coal during continuous operation [34]. Afterwards, this oxygen carrier was evaluated by means of continuous tests in a CLC rig burning differently ranked coals [35] and during biomass combustion [36]. Complete fuel combustion was always achieved, although the mechanical strength of the oxygen carrier particles decreased during the operation in the CLC unit [37].

Furthermore, the high cost of copper oxide can be seen as another disadvantage, so it would seem reasonable to decreasing the CuO weight percentage. In this sense, Pérez-Vega et al. [38] replaced 10 % the CuO in the material comprising 60 % CuO supported on $MgAl_2O_4$ with Fe_2O_3, while always achieving complete coal combustion. Additionally, the substitution of CuO by manganese oxide has been evaluated through discontinuous tests. Pour et al. [39] analyzed the Cu:Mn molar ratio, and observed that mechanical properties decreased in proportion with the decrease in the amount of CuO. Hosseini et al. [40] found a material with a Mn:Cu ratio of 25:75 that has improved characteristics compared to those of the single metal oxide. Adánez-Rubio et al. [41] found a suitable oxygen carrier with a Cu:Mn ratio of 34:66 that retained adequate mechanical strength and a low attrition rate

after 45 h of operation. This oxygen carrier showed excellent performance in a CLOU unit burning coal, while the evolution of its mechanical properties depended on the solids circulation rate [42]. Thus, particles maintained high mechanical strength when the solids circulation rate was high enough to support an oxygen carrier to fuel ratio higher than 3-4.

In order to obtain an ever more economical oxygen carrier for CLOU process, the search for other Cu-free materials based mainly on manganese oxides with oxygen uncoupling capability has been promoted. Among these materials, the oxygen carriers based on CaMn-perovskites [43], materials based on Mn-Si [44], and the solids formed by combining manganese-iron oxides [45] are worthy of note. The use of both CaMn-based perovskites [46] and Mn-Si mixed oxide particles [47] showed improved performance compared to *i*G-CLC when they were tested in CLC units, although not as good as the performance shown by Cu-based materials. Nevertheless, CaMn-based perovskite oxygen carriers were highly sensitive to the presence of sulfur [43,48], and are mainly proposed for the combustion of sulfur-free fuels such as biomass [49]. Oxygen carriers comprising Mn-Fe mixed oxides have received the most attention from several research groups for the development of materials with oxygen uncoupling capability.

1.2. State of development of manganese-iron mixed oxides as oxygen carrier material

Mn-Fe mixed oxides are capable of generating an oxygen-gas phase through the chemical decomposition of bixbyite [$(Mn_xFe_{1-x})_2O_3$] to spinel [$(Mn_xFe_{1-x})_3O_4$], through reaction R1. Azimi et al. [50] indicated that oxygen uncoupling capability was enhanced in Mn-rich materials owing to the thermodynamics of the Mn-Fe-O system. Mugse et al. [51] observed that bixbyite was always regenerated by oxidation of the spinel phase through long air

exposure times. However, Shafiefarhood et al. [52] considered that the increase in the amount of manganese in the mixed oxides hindered oxidation from spinel to bixbyite when the partial pressure of oxygen was low. This is in agreement with the Lambert et al. [53], who observed that bixbyite regeneration reaction kinetics was always very slow for Mn-rich solids. Consequently, Larring et al. [54] postulated that in order to take advantage of the oxygen release capability of these materials, an exhaustive control of oxidation conditions, i.e., temperature and partial pressure of oxygen, is essential. Taking this into account, Pérez-Vega et al. [55] delimited operating temperature range for the CLOU process of a Mn-rich oxygen carrier selected after a screening process. The authors determined that it would be necessary set a thermal gradient of about 70 ºC between the reactors in order to take advantage of the oxygen uncoupling properties of the solid. Finally, Abián et al. [56] studied the influence of the Mn:Fe ratio on the decomposition and regeneration rates of bixbyite. They found that mixing similar amounts of the manganese and iron oxides produced the highest spinel oxidation rate.

Furthermore, Lambert et al. [53] observed that a higher fraction of oxygen can be active when the solid reacts with a reducing gas, e.g., H_2, CO or CH_4, making it possible to reduce the spinel to mangano-wüstite [$(Mn_xFe_{1-x})O$] in the basic CLC process; see reactions R2-R4. This redox system, i.e., $(Mn_xFe_{1-x})_3O_4/(Mn_xFe_{1-x})O$, was exploited by Wang et al. [57] to burn coal in a thermogravimetric analyzer (TGA). In addition, mangano-wüstite could further be reduced to metallic iron, although this is not advised owing to thermodynamic restrictions in order to fully oxidize the fuel to CO_2 and H_2O [58].

$$3\,(Mn_xFe_{1-x})_2O_3 \leftrightarrow 2\,(Mn_xFe_{1-x})_3O_4 + 0.5\,O_2 \quad \text{(R1)}$$

$$(Mn_xFe_{1-x})_3O_4 + H_2 \leftrightarrow 3\,(Mn_xFe_{1-x})O + H_2O \quad \text{(R2)}$$

$$(Mn_xFe_{1-x})_3O_4 + CO \leftrightarrow 3\,(Mn_xFe_{1-x})O + CO_2 \quad (R3)$$

$$4\,(Mn_xFe_{1-x})_3O_4 + CH_4 \leftrightarrow 12\,(Mn_xFe_{1-x})O + CO_2 + 2\,H_2O \quad (R4)$$

With regard to the evaluation of Mn-Fe mixed oxide materials, most of the works were focused on the study of the reactivity of the oxygen uncoupling reaction and mechanical strength of particles in batch mode apparatuses, e.g., TGA, or batch fixed or fluidized bed reactors. Limited works have been found in relation to the use of these materials for burning a fuel in a CLC unit. Along these lines, Rydén et al. used Mn-Fe [59] and Mn-Fe-Ti [60] materials in a 300 W_{th} CLC unit to burn methane. Good conversion was obtained with the Mn-Fe material, but the lifetime of the particles was extremely short. On the contrary, low methane conversion was achieved with the Mn-Fe-Ti because of its low reactivity, while quite moderate particle attrition was also observed.

In light of the results obtained with Mn-Fe oxygen carriers, it is clear that materials of a high mechanical strength must be developed for use in CLC unit operations, while high reactivity must be maintained in order to achieve high fuel conversion. In a previous study, a promising low-cost MnFe-based oxygen carrier, $(Mn_{0.77}Fe_{0.23})_2O_3$, was found after a screening process on particles prepared by mechanical mixing followed by pelletization [55]. This solid was evaluated in both a TGA and a fluidized bed reactor, and it was found to possess the reactivity and mechanical strength required for use in a CLC unit.

1.3. Objective

The objective of this work was to evaluate a $(Mn_{0.77}Fe_{0.23})_2O_3$ solid prepared by an industrial method as an oxygen carrier for use in a CLC unit burning gaseous or solid fuels. For this purpose, $(Mn_{0.77}Fe_{0.23})_2O_3$ particles were obtained by spray drying. The preparation

method was optimized to achieve suitable values of crushing strength, oxygen transport capacity, and rate index. Rate index is a gauge of reactivity, indicating rated of reaction of oxygen carrier particles. Both CLOU and CLC processes were assessed. Finally, the performance of the oxygen carrier with syngas, methane and coal was evaluated in two CLC units.

2. Experimental section

Following, the experimental method is described, including a description of the materials and facilities used, as well as the experimental procedure.

2.1. Preparation of the oxygen carrier particles

The MnFe-based oxygen carrier particles were manufactured in a spray drier placed at the Flemish Institute for Technological Research (VITO) following our instructions. A detailed description of the procedure developed to obtain the spray-dried particles can be consulted elsewhere [50]. The $(Mn_{0.77}Fe_{0.23})_2O_3$ particles, here named Mn77Fe[SD], were prepared with the same composition (76 wt.% Mn_3O_4 and 24 wt.% Fe_2O_3), particle size (100-300 μm), and sintering conditions (4 h at 950 ºC) as the material previously prepared by mechanical mixing [55].

2.2. Physical characterization of the spray-dried particles

Physical characterization was performed by applying different techniques. The main crystalline phases were determined by X-ray powder diffraction (XRD) patterns acquired in

a Bruker AXS D8 Advance X-ray diffractometer equipped with an X-ray source with a Cu anode working at 40 kV and 40 mA and an energy-dispersive one-dimensional detector. The assignment of crystalline phases was carried out by means of Join Committee on Powder Diffraction Standards (JCPDS) database using DIFFRAC.EVA software. The quantification of the chemical species in the crystalline part of the solid was performed by means of TOPAS software. The magnetism of the particles was evaluated by means of relative permeability (K_m) by measuring magnetic susceptibility. These measurements were performed using a Bartington Instruments MS3 magnetic susceptibility meter from coupled with an MS2G single frequency sensor. Detailed information on the determination of K_m was already given by Abián et al. [56].

Crushing strength was determined using a Shimpo FGN-5X force gauge, taking the average value of 20 measurements of the force needed to fracture a particle. Attrition resistance values were determined by means of the Air Jet Index (AJI) using a three-hole air jet attrition tester ATTRI-AS (Ma. Tec. Materials Technologies Snc.) in agreement with the ASTM-D-5757-11 standard [61]. The attrition rate and lifetime of the oxygen carrier in continuous CLC tests was measured taking into account the methodology suggested by Cabello et al. [62]. Particle size distribution was obtained in a Beckman Coulter LS13320 particle size analyzer by applying the laser diffraction technique (ISO13320 standard). Porosity was measured by Hg intrusion in a Quantachrome PoreMaster 33.

2.3. Chemical characterization in a thermogravimetric analyzer

The oxygen transport capacity (R_{OC}) and the reactivity of calcined and cycled particles were determined using a TGA, CI Electronics type. Approximately 50 mg of sample was

placed in a platinum basket suspended inside a quartz reactor. First, the particles were heated in air to the desired temperature. Four consecutive redox cycles were then conducted to analyze their behavior in both CLOU and CLC modes.

Oxygen uncoupling capability was evaluated during the decomposition-regeneration of the bixbyite phase by alternating high-purity N_2 (< 2ppm O_2) and air at 870 ºC, in a way similar to that described in a previous work [55]. In addition, reactivity with H_2, CO and CH_4, as well as oxidation by O_2, was assessed during the reduction of spinel to mangano-wüstite. Redox cycles were performed alternating the gaseous fuels and air at 950 ºC. H_2O or CO_2 was included in the reaction mixture flow to prevent the reduction of iron compounds to FeO or Fe, which is undesirable if complete fuel oxidation is to be achieved.

Oxygen transport capacity for oxygen uncoupling (R_{OC}^{ou}) and gas-solid reaction (R_{OC}^{g}) were calculated by Eq. 1:

$$R_{OC}^{i} = \frac{m_o^i - m_r^i}{m_{bix}} \quad (1)$$

where m_o^i and m_r^i are the mass of the oxidized and reduced sample, respectively. For oxygen uncoupling, R_{OC}^{ou} was calculated considering the mass m_o^{ou} achieved after the oxidation period and the mass m_r^{ou} of the sample in the spinel form; see reaction R1. For the reduction with a fuel gas, R_{OC}^{g} was calculated considering m_o^g as the mass of the sample in spinel form and m_r^g the mass of the sample after the reduction period following reaction R2-R4. m_{bix} is the mass of the sample assuming full oxidation to bixbyite. In this way, the total oxygen transport capacity of the solid by reduction from bixbyite to mangano-wüstite can be calculated by $R_{OC}^{t} = R_{OC}^{ou} + R_{OC}^{g}$.

The reactivity of the particles was calculated through the normalized rate index values determined by applying Eq. 2:

$$Rate\ index\ (\%/\min) = 60 \cdot 100 \cdot \frac{P_{ref}}{P_{TGA}} \frac{1}{m_o} \left(\frac{\mathrm{d}m}{\mathrm{d}t} \right) \quad (2)$$

where P_{TGA} is the partial pressure of the reacting gas in TGA; P_{ref} is the reference partial pressure of the reacting gas (0.15 atm for the reduction and 0.10 atm for the oxidation; the quotient P_{ref}/P_{TGA} was not considered for oxygen uncoupling); m_0 is the initial mass of the sample; and m is the mass of oxygen carrier. The reaction rate $\left({}^{dm}/_{dt} \right)$ was calculated at the beginning of the reaction.

2.4. Characteristics of the coals used

Four different coals, covering a wide rank of coals, were used for CLC tests, in a continuous facility: an anthracite (ANT) from the Bierzo basin (Spain), a bituminous South African coal (BIT), a lignite (LIG) from the Teruel basin (Spain), and a subbituminous coal (SUB) from "Mina Invierno" in Chile. The diameter of the coal particles was +200-300 μm. The main characteristics of the coals are shown in Table 1. The oxygen demand for each coal (Ω_{SF}) represents the stoichiometric mass of oxygen needed for full coal combustion.

Table 1. Properties of the coals used (humidity stabilized by exposure to the atmosphere).

	ANT	**BIT**	**LIG**	**SUB**
Proximate analysis (wt.% raw matter)				
Moisture	1.0	3.5	12.5	14.8
Volatile matter	7.6	25.5	28.7	33.1
Fixed carbon	59.9	55.3	33.6	36.1
Ash	31.5	15.7	25.2	16.0
Ultimate analysis (wt.% raw matter)				
C	60.7	66.3	45.4	51.5

H	2.1	3.6	2.5	3.4
N	0.9	1.8	0.6	0.7
S	1.3	0.5	5.2	0.3
O[(1)]	2.5	8.6	8.6	13.3
LHV (kJ/kg coal)	21880	24930	16250	18680
Ω_{SF} (kg O/kg coal)	1.8	2.0	1.4	1.5

(1) Oxygen by difference.

2.5. Description of chemical looping facilities

Two CLC units, ICB-CSIC-g1 and ICB-CSIC-s1, were used to evaluate the performance of the MnFe-based oxygen carrier throughout the CLC process during both fuel gas and coal combustion, respectively. Diagrams showing the layout of these facilities are provided in Figure 1, and the main design parameters are included in Table 2. Both facilities consist of two interconnecting bubbling fluidized bed reactors as fuel and air reactors connected by a loop seal. The upper part of the air reactor was designed as a narrow and long riser to guarantee an adequate flow of solids from the air reactor to the fuel reactor. In addition, the rigs are equipped with a solids device to measure the solids circulation flow and a solids control valve to vary the solids circulation rate between the reactors. A more detailed description can be found elsewhere for the ICB-CSIC-g1 unit [10] and the ICB-CSIC-s1 pilot plant [63].

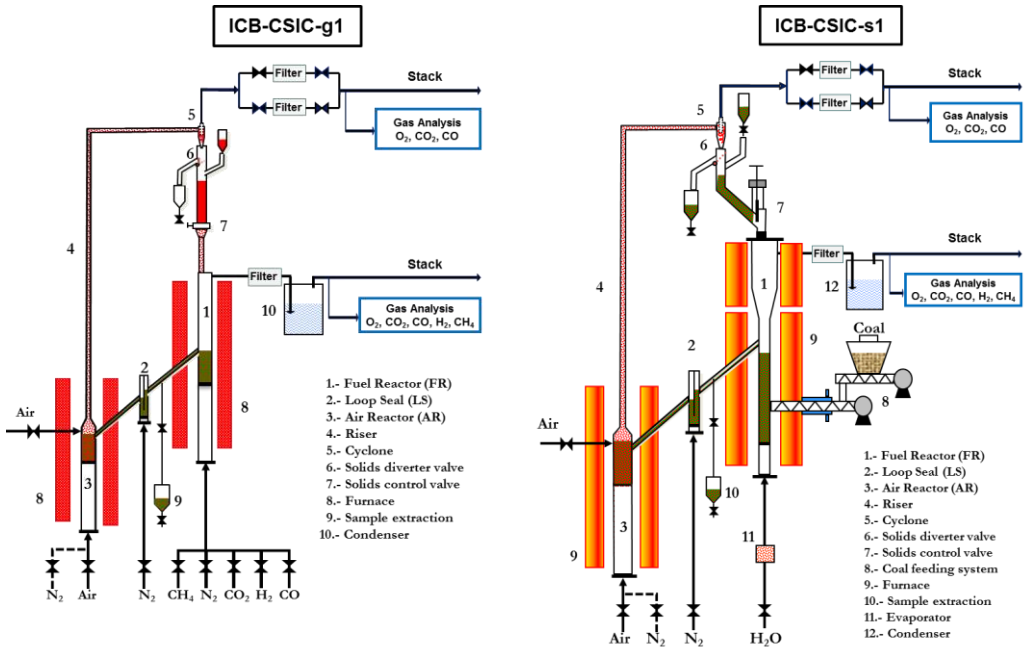

Figure 1. Layout of the 500 W_{th} CLC facilities: ICB-CSIC-g1 for gaseous fuels and ICB-CSIC-s1 for solid fuel.

Table 2. Main dimensions of CLC facilities.

		ICB-CSIC-g1	ICB-CSIC-s1
Fuel Reactor	Diameter (m)	0.05	0.05
	Bed height (m)	0.10	0.20
Air Reactor	Diameter (m)	0.05	0.08
	Bed height (m)	0.10	0.10

Two batches of 2 and 3 kg of oxygen carrier particles were prepared for use during the fuel gas and coal combustion tests, respectively, in order to characterize the cycled particles as a function of both the fuel and operating conditions. Thus, 1.6 kg was introduced into the ICB-CSIC-g1, whereas 2.6 kg was used in the ICB-CSIC-s1, with the differences in the solids inventory justified by the dimensions of each unit; see Table 2.

The concentration of the main gases in the outlet streams of the fuel reactor (CO_2, CO, H_2, CH_4 and O_2) and air reactor (O_2, CO_2 and CO) was analyzed after gas drying. CO_2, CO and

CH_4 concentration values were measured by a non-dispersive infrared (NDIR) analyzer (Siemens Ultramat 23); H_2 concentration was measured by a thermal conductivity detector (Maihak S710/THERMOR); and O_2 concentration was obtained using a paramagnetic analyzer (Siemens 23/Oxymat 6).

2.6. Experimental procedure and data evaluation

Syngas and methane as fuel gas were fed into the ICB-CSIC-g1 unit and four different coals were used in the ICB-CSIC-s1 unit. Table 3 shows the operating conditions set in both facilities. Seven tests were carried out in ICB-CSIC-g1 burning either syngas (S1-S3) or methane (M1-M4). The fuel reactor inlet flow was set at 156 NL/h (gas velocity of 0.09 m/s at 900 ºC). The syngas was formed by a CO:H_2 ratio of 3:1 representing 60 vol.% of the total gas supplied to the fuel reactor. In addition, CO_2 (15 vol.%) and N_2 (to balance) were fed together mixed with the CO-H_2 in order to prevent carbon deposition during the combustion. The CH_4 concentration introduced into the fuel reactor was set at 25 vol.% (N_2 to balance). Air was supplied to the air reactor divided into two streams: 720 NL/h was fed into the bottom part and 150 NL/h was introduced into the upper part (riser). The fuel reactor temperature was varied in order to evaluate its effect on fuel conversion. The air reactor temperature was maintained in the 930-940 ºC interval in all tests. In total, the oxygen carrier spent 20 h circulating in hot conditions between the air and fuel reactors, 10 h of which corresponded to fuel gas combustion.

Table 3. Operating conditions set in both ICB-CSIC-g1 and ICB-CSIC-s1 with Mn77Fe[SD] oxygen carrier.

Facility	Fuel	Test	Operating conditions				
			T_{FR} (ºC)	$\dot{m}_{OC}$ (kg/h)	m^*_{OC} (kg/MW_{th})	ϕ [(a)] (–)	Power (W_{th})
ICB-CSIC-g1	Syngas	S1	910	4.7	2004	4.2	330
		S2	930	4.7	2125	4.2	330
		S3	965	5.5	2186	5.0	330
	CH_4	M1	905	4.8	1282	2.9	422
		M2	925	4.8	1234	2.9	422
		M3	940	4.7	1329	2.8	422
		M4	965	4.8	1424	2.9	422
ICB-CSIC-s1	ANT	C1	905	2.3	1374	1.0	511
	BIT	C2	900	2.6	1276	1.0	644
	LIG	C3	900	2.6	1564	1.1	474
	SUB	C4	900	2.8	1755	1.5	446

[(a)] ϕ: oxygen carrier to fuel ratio, calculated as the flow of oxygen in the oxygen carrier stream (assumed in its fully oxidized state) divided by the stoichiometric flow of oxygen required to burn the fuel [10,62].

In the tests performed burning coal in ICB-CSIC-s1 (C1-C4), steam was used as the gasifying and fluidizing agent in the fuel reactor. The steam flow supplied was set at 130 NL/h (gas velocity of 0.08 m/s at 900 ºC). An air flow of 2400 NL/h was fed into the bottom part of the air reactor, corresponding to a gas velocity in the bottom of 0.6 m/s and in the riser of 4 m/s at 900 ºC. The operating conditions were chosen to be similar to those used in previous experiments conducted in this CLC unit burning the same coals, but using ilmenite [64], an iron-based waste product (Fe-ESF) [63] or an iron ore (Fe-ore) [65] as the oxygen carrier. This allowed the performance of the different oxygen carrier materials in CLC with coal to be compared. In total, the material was subjected to 20 h of continuous hot circulating, 10 h of which corresponded to coal combustion.

The performance of the CLC process with coal was evaluated by means of two parameters: CO_2 capture efficiency and total oxygen demand. CO_2 capture efficiency (η_{CC}) is defined as the fraction of carbon converted to gas in the fuel reactor with respect to the total carbon converted into the CLC unit:

$$\eta_{CC} = \frac{\left(F_{CO_2} + F_{CO} + F_{CH_4}\right)_{outFR}}{\left(F_{CO_2} + F_{CO} + F_{CH_4}\right)_{outFR} + \left(F_{CO_2}\right)_{outAR}} \quad (3)$$

where $(F_i)_{out\ j}$ represents the molar flow of each compound *i* in the exit stream of each reactor (*j*= FR or AR).

Total oxygen demand (Ω_T) is defined as the fraction of the stoichiometric oxygen required by the fed fuel to fully oxidize the unburned gases exiting from the fuel reactor. It gives a clear idea of the amount of oxygen that should be supplied in an oxygen polishing unit.

$$\Omega_T = \frac{\left(4F_{CH_4} + F_{CO} + F_{H_2}\right)_{outFR}}{F_{O,\ fuel}} \quad (4)$$

where $F_{O,\ fuel}$ is the stoichiometric molar flow of atomic oxygen needed to oxidize the fuel to CO_2 and H_2O.

In the fuel gas combustion tests, performance of the CLC process was evaluated by means of combustion efficiency in the CLC unit (η_{comb}) calculated by Eq. 5:

$$\eta_{comb} = 1 - \Omega_T = 1 - \frac{\left(4F_{CH_4} + F_{CO} + F_{H_2}\right)_{outFR}}{F_{O,\ fuel}} \quad (5)$$

At this point, it must be considered that CO_2 capture efficiency does not evaluate if all carbon-based gaseous compounds exiting from the fuel reactor are in form of CO_2. This issue is evaluated by means of combustion efficiency and/or oxygen demand. In fact, CO_2 capture concept assumes that all carbon exiting from the fuel reactor is potentially captured into the CLC unit [21]. Thus, when an incomplete combustion was observed into the fuel reactor, an additional post-treatment with pure oxygen, e.g., an oxygen polishing step, would be required in order to complete the oxidation of the unconverted compounds [21]. For example, during the combustion of gaseous fuel, no carbon in the air reactor was observed. This means that CO_2 capture of 100 % can be potentially achieved even if uncomplete combustion was observed.

To calculate each evaluated parameter (η_{CC}, Ω_T, and η_{comb}) for the combination of operating conditions set in each test (see Table 3) a steady state was reached that lasted around 1 h. During this period the concentration values for CO_2, CO, H_2 and CH_4 in the fuel reactor and for CO_2 and O_2 in the air reactor were roughly constant. The molar flow of the gaseous compounds exiting from the reactors, required to calculate η_{CC}, Ω_T and η_{comb} (see Eqs. 3, 4 and 5), was estimated by finding the concentration of every gas and the N_2 flow [21].

3. Results and discussion

Oxygen carrier particles must possess several characteristics to be used in chemical looping processes, including high reactivity and mechanical strength, as well as avoidance of agglomeration. Following, the preparation method is optimized by a trade-off between reactivity and mechanical strength, before the selected particles were used in CLC units to burn gaseous and solid fuels.

3.1. Oxygen carrier physicochemical characterization

Figure 2 shows the rate index and the oxygen transport capacity values of the MnFe-based particles prepared by spray drying as received (i.e., calcined at 950 ºC).

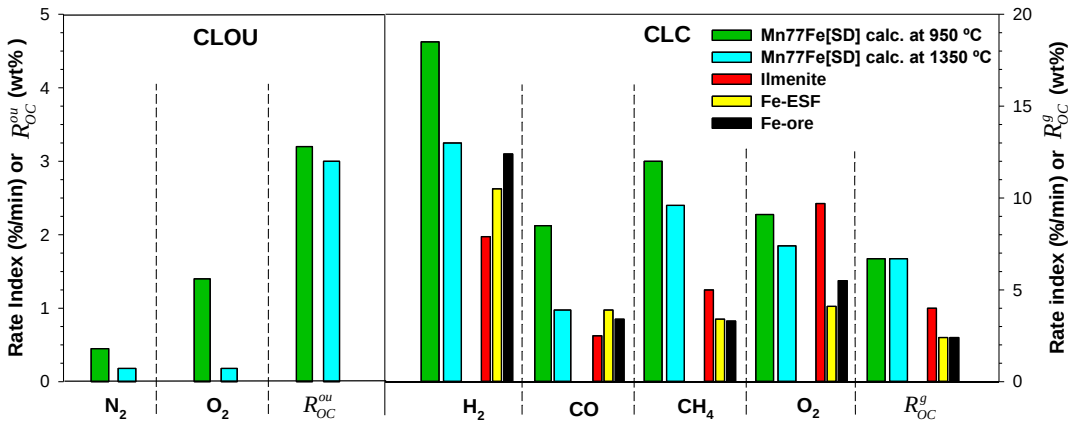

Figure 2. Rate Index with different gases and oxygen transport capacity values of Mn77Fe[SD] particles calcined at 950 and 1350 ºC. Data for other low-cost Fe-based oxygen carriers tested in *i*G-CLC have been also included for comparison purposes [66].

Mn77Fe[SD] particles showed high reactivity for reduction of spinel with fuel gases as well as for the oxidation of mangano-wüstite in CLC mode. In fact, the rate index with H_2, CO and CH_4 was higher than those shown for materials previously considered as oxygen carriers for coal combustion, i.e., ilmenite, Fe-ESF, and Fe-ore. Also, this material showed a high value for the oxygen transport capacity in CLC mode, R_{OC}^{g} = 6.7 wt.%, which is the theoretical value for the reduction of spinel to mangano-wüstite [55]. In addition, the Mn77Fe[SD] material calcined at 950 ºC showed relevant oxygen uncoupling properties. In fact, the main phase identified by XRD in the calcined particles was bixbyite; see Table 4. During nitrogen-air cycles, the material could be easily oxidized to bixbyite, which could be chemically decomposed to spinel in the inert atmosphere. The fraction of oxygen supplied by the oxygen uncoupling mode was R_{OC}^{ou} = 1.4 wt.%. In spite of its good chemical properties, its particles had low mechanical strength (crushing strength was 0.4 N), was an

unsuitable value for use in a CLC unit [62]. It should be noted that a crushing strength value of well above 1 N is recommended in order for a material to be considered suitable.

In order to increase their mechanical strength, particles were further calcined for 2 hours at different temperatures (1100-1350 ºC). Table 4 shows the results observed after the physical characterization of the different spray-dryied particles.

Table 4. Physical features of Mn77Fe[SD] particles as a function of calcining temperature.

			Sintering temperature (ºC)				
			950	1100	1200	1250	1350
Crushing strength (N)			0.4	0.4	0.4	1.2	1.7
Porosity (%)			59.6	50.2	45.3	26.8	19.0
Relative permeability (-)			1.0	1.0	1.0	2.7	2.5
XRD main phases (%)	Bixbyite	Mn_2O_3	55.1	54.4	54.2	20.8	6.4
		$MnFeO_3$	44.9	45.6	45.8	-	-
		$Mn_{0.7}Fe_{0.3}O_3$	-	-	-	6.4	7.2
		Total phases	100.0	100.0	100.0	27.2	13.6
	Spinel	Mn_2FeO_4	-	-	-	5.2	10.9
		$Mn_3Fe_3O_8$	-	-	-	19.2	23.8
		$Mn_{1.58}Fe_{1.42}O_4$	-	-	-	12.0	16.9
		Mn_3O_4	-	-	-	36.8	34.8
		Total phases	0.0	0.0	0.0	72.8	86.4

The crushing strength of the particles was increased with the rise in the sintering temperature above 1200 ºC, as was intended. Calcination at 1350 ºC produced particles with a crushing strength value well above the threshold value (1 N). It is clear that the rise in the mechanical resistance with the calcining temperature is directly related to the loss of porosity in the particles. In addition, sintering temperatures higher than 1200 ºC led to a change in the crystallinity of the solid, which presented a higher proportion of $(Mn_xFe_{1-x})_3O_4$ phases. During the heating of the particles, only spinel phases were formed [67],

which could subsequently be oxidized to bixbyite phases during slow cooling in air. This fact is clearly shown in the particles calcined in the 950-1200 ºC interval. However, a higher sintering temperature could reduce the oxidation rate, preventing oxidation to the bixbyite phases. It is well known that manganic ferrites forming spinel phases show relevant magnetic properties [68]. Thus, magnetic behavior was observed in the particles calcined at 1250 ºC and 1350 ºC, where the increase in the spinel phases was observed; see K_m parameter in Table 4. This property is highly relevant for the use of this material in the CLC of coal, as magnetic oxygen carrier could be easily separated from ash in the purge stream for reuse in the CLC unit.

Higher calcining temperature barely affected to the oxygen transport capacity for both CLC and CLOU; see R_{OC}^{g} and R_{OC}^{ou} in Figure 2. However, the calcining process affected the reactivity of the material. With regard to the CLOU process, the material calcined at 1350 ºC needed double the time during the oxygen uncoupling period and 10 times the oxidation time in order to complete the reaction in the TGA. Consequently, perticles calcined at 1350 ºC were found to have a low reaction rate during the chemical decomposition of bixbyite and oxidation of the spinel phase, which caused a severe decrease in the oxygen uncoupling ability. For the processes involved in CLC, a relevant decrease was also observed in the reduction with H_2 and CO, but only minor differences were found for the reduction with CH_4 and oxidation of mangano-wüstite to spinel. Even so, the rate indices of the Mn77Fe[SD] material calcined at 1350 ºC were higher than or similar to those found for other reference materials.

After physical and chemical characterization, it could be affirmed that Mn77Fe[SD] particles sintered at 1350 ºC achieved the required crushing strength to be used in CLC.

Reactivity and oxygen transport capacity with gaseous fuels were maintained in adequate values to consider the use of this oxygen carrier in CLC with *ex-situ* or *in-situ* gasification of coal. Its highly relevant is the high reactivity with CH_4, compared to other materials used in CLC with coal, is of great relevance, given that this would increase the combustion efficiency of the process because a large proportion of the oxygen demand comes from unconverted CH_4 [21]. In addition, the oxygen transport capacity of the Mn-Fe mixed oxide was notably greater than that of the other oxygen carriers. Thus, the solids circulation rate required to transport a definite flow of oxygen would be lower than with other materials, which would increase the residence time of solids in the fuel reactor, facilitating char conversion and eventually improving the CO_2 capture. Moreover, the magnetic capacity of the Mn77Fe[SD] particles calcined at 1350 ºC can be considered an additional improvement for an oxygen carrier in *i*G-CLC with coal. However, its oxygen uncoupling ability was highly reduced, preventing its use for CLOU. Therefore, the performance of Mn77Fe[SD] calcined at 1350 ºC was evaluated in continuously operated CLC facilities with fuel gases and coal in the *i*G-CLC mode.

3.2. Performance of the oxygen carrier with fuel gases

The performance of Mn77Fe[SD] in CLC with gaseous fuels was evaluated by means of experiments carried out at the ICB-CSIC-g1 CLC facility; see Figure 1 and Table 3. Figure 3 shows the combustion efficiency with syngas in tests S1-S3. Combustion efficiency was 96 % at 910 ºC in the fuel reactor, and complete combustion was achieved at 930 ºC. Thus, its use seems to be advisable for the syngas combustion at a suitable temperature higher than 900 ºC.

Some tests were also conducted with CH_4, considering the relatively high reactivity of this material for this gas; tests M1-M4. The combustion efficiency of CH_4 increased with temperature in the fuel reactor from a poor value of 48 % at 905 ºC up to 78 % at 965 ºC. From results shown in Figure 3, close to full combustion of CH_4 would be expected at temperatures above 1000 ºC. Unfortunately, this high temperature was not achieved in the CLC unit because of the heat losses associated with the small scale of the CLC unit. This behavior is similar to that found for an Fe-based oxygen carrier [12].

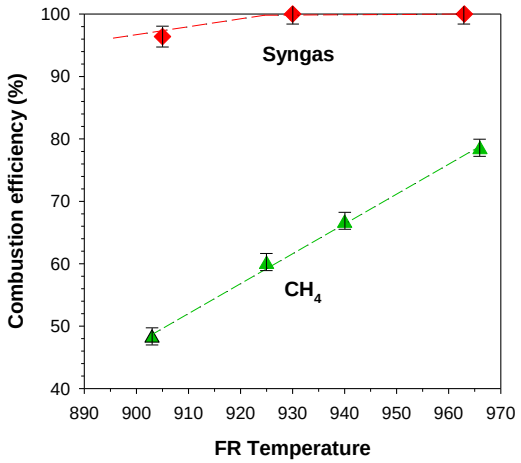

Figure 3. Combustion efficiency vs. fuel reactor temperature during the combustion of gaseous fuels (tests S1-S3 and M1-M4).

In addition, it is relevant that during the periods where no fuel was fed into the system, no oxygen was found at the fuel reactor exit, nor was any oxygen consumption observed in the air reactor. Thus, the Mn77Fe[SD] material calcined at 1350 ºC did not show any oxygen uncoupling capability under the conditions used in the CLC unit. This agrees with the difficulty encountered in oxidizing the spinel to bixbyite observed during particles characterization; see Section 3.1. It can therefore be deduced that conversion of any fuel gas is the result of the gas-solid reaction between the fuel and the oxygen carrier particles.

1

2 3.3. Performance of the oxygen carrier with coal

3 The Mn77Fe[SD] material was also used to burn coal in the 500 W_{th} ICB-CSIC-s1; see
4 Figure 1. Four coals were used, three of which (ANT, BIT and LIG) had already been used
5 in this CLC unit with others low-cost Fe-based materials (i.e., ilmenite [64], Fe-ESF [63]
6 and Fe-ore [65]). Similar operating conditions to those used in previous works were
7 selected in this work in order to obtain reliable a comparable results. The performance of
8 *i*G-CLC with Mn77Fe[SD] burning coal was evaluated by CO_2 capture efficiency (η_{CC}) and
9 total oxygen demand (Ω_T); see Figures 4 and 5.

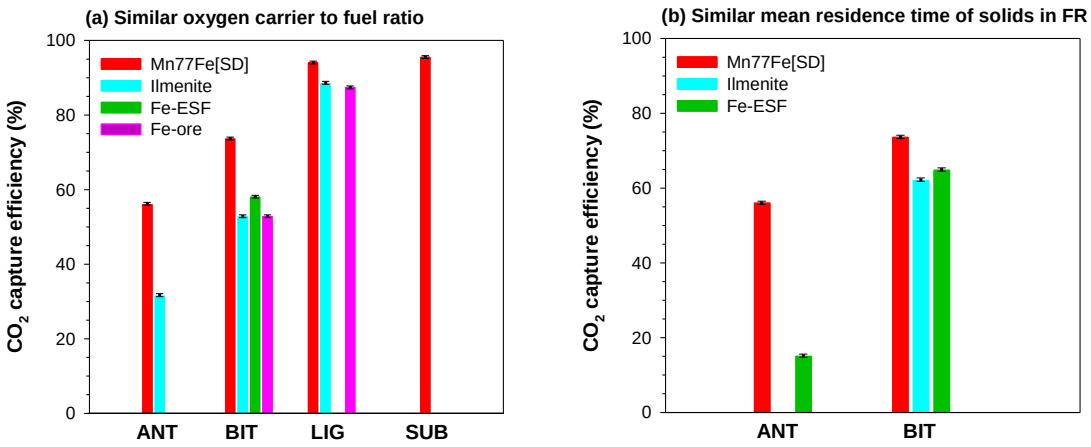

10

11 **Figure 4**. CO_2 capture efficiency achieved by burning different coals with Mn77Fe[SD]
12 calcined at 1350 ºC. Results obtained with other oxygen carrier materials are included for
13 comparison purposes [63-65]. T_{FR} ~ 900 ºC.

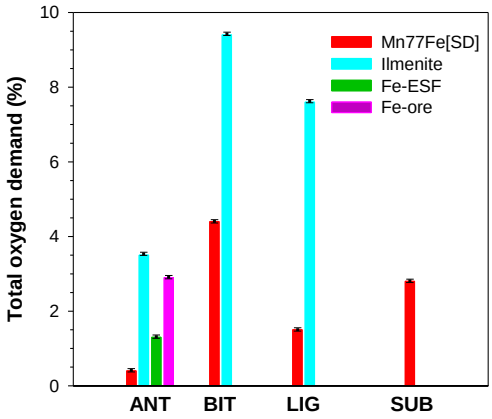

Figure 5. Total oxygen demand for different coals with Mn77Fe[SD] calcined at 1350 ºC. Results obtained with other oxygen carrier materials are included for comparison purposes [63-65], Oxygen carrier to fuel ratio ($\phi \approx 1$). $T_{FR} \approx 900$ ºC.

With Mn77Fe[SD], the highest CO_2 capture efficiency values were achieved with subbituminous coal and lignite (95.5 and 94.1 %, respectively); see Figure 4. CO_2 capture was lower with the bituminous coal and anthracite (73.6 % and 56.0 %, respectively). CO_2 capture with solid fuels mainly depended on the reactivity of the solid fuel and the mean residence time of the solids in the fuel reactor [21]. In these tests, the mean residence time of solids were maintained in the 17-18 min interval; thus, differences in CO_2 capture were mainly due to the different char gasification rate for every coal [63,69].

Total oxygen demand varied between 0.4 % with the anthracite and 4.4 % with the bituminous coal; see Figure 5. Differences in oxygen demand with the type of solid fuel could be assigned to the different fraction of volatile matter in every coal used, but also to different operating conditions used. Thus, it had previously been determined that the main unconverted products exiting this unit, where the fuel reactor is in the bubbling fluidization

regime, proceeded from the volatile matter [70]. Therefore, the lowest oxygen demand value was observed with the anthracite because it is the coal with the lowest fraction of volatile matter; see Table 1. Oxygen demand was highest for the bituminous coal, which was used at similar operating conditions as those for anthracite; see Table 3. However, lower total oxygen demand values (1.5 and 2.8 %) were obtained with lignite and subbituminous coal compared to those of the bituminous coal, although their fraction of volatile matter was higher. In this case, the higher specific solids inventory in the fuel reactor and/or the higher oxygen carrier to fuel ratio, ϕ, used during the combustion of lignite and subbituminous coal could may have contributed to the lower total oxygen demand. It should be noted that the specific solids inventory in the fuel reactor and ϕ parameter had been identified as the operating conditions with greatest influence on total oxygen demand [21].

The CO_2 capture and total oxygen demand values obtained with the MnFe-based material and other low-cost Fe-based solids in the same ICB-CSIC-s1 facility were compared. Figure 4(a) shows CO_2 capture for conditions at which values of both the oxygen carrier to fuel ratio and specific solids inventory in the fuel reactor would be similar. Higher CO_2 capture efficiency was achieved with Mn77Fe[SD] regardless of the coal burned. Small differences were observed during lignite combustion with respect to the tests using ilmenite and Fe-ore because of the high gasification rate of this coal, which yielded high CO_2 capture in all cases. However, greater differences were obtained with the other coals because CO_2 capture was highly limited by the char conversion rate. Under these conditions, the mean residence time of solids in the fuel reactor was affected by the different oxygen transport capacity of every material; see Table 5. It should be noted that an

oxygen carrier with lower oxygen transport capacity requires a higher circulation rate to achieve the same oxygen carrier to fuel ratio [17]. Thus, differences in the CO_2 capture may be the result of the different mean residence time of solids in the fuel reactor [21].

Table 5. Oxygen transport capacity of different oxygen carriers and its effect on: (1) the mean residence time of solids in the fuel reactor, τ_{OC}, considering the same ϕ value; and (2) the ϕ ratio considering the same solids circulation rate.

	R_{OC}^{g} (%)	τ_{OC} [(a)] (min)	ϕ [(b)](–)
Mn77Fe[SD]	6.7	18.0	1.00
Ilmenite	4.0	10.7	0.60
Fe-ESF	2.0	5.4	0.30
Fe-ore	2.5	6.7	0.37

[(a)] To achieve the same ϕ value at similar specific solids inventory
[(b)] Equal solids circulation rate

However, a CLC unit would be designed to operate with a fixed solids circulation rate. To evaluate the real potential of Mn77Fe[SD] on *i*G-CLC with coal, Figure 4(b) shows the CO_2 capture achieved with different oxygen carriers and fuels in experiments where the solids circulation rate was the same, which implies solids having the same mean residence time in the fuel reactor. There were fewer differences in CO_2 capture between different oxygen carriers than when considering the ϕ parameter constant, as the mean residence time of solids was increased for ilmenite, Fe-ESF, and Fe-ore to 18 min with respect to experiments shown in Figure 4(a). In spite of this, the highest CO_2 capture was achieved with Mn77Fe[SD] in all cases.

In addition, the lowest total oxygen demand values were always reached with the Mn-Fe material regardless of the coal used; see Figure 5. This was due to the higher rate index values of the spray-dryied particles; see Figure 2. Experiments were selected in order to

have similar values of both oxygen carrier to fuel ratio and specific solids inventory in the fuel reactor, except for Fe-ESF with anthracite, where the solids inventory was about 2200 kg/MW_{th}. Such a high solids inventory would be the reason for the lower oxygen demand when compared to the other low-cost Fe-based oxygen carriers. However, the oxygen demand was lower with Mn77Fe[SD], even though a lower specific solids inventory was used in the fuel reactor.

With regard to the relevance of using the Mn77Fe[SD] material for oxygen demand, the case in which the solids circulation rate is constant must be also considered. In this case, the oxygen carrier to fuel ratio value decreased as the oxygen transport capacity was reduced; see Table 5. Logically, total oxygen demand should have been higher as the oxygen carrier to fuel ratio decreased when compared to the results shown in Figure 5 [21]. For example, the total oxygen demand with Fe-ore and anthracite was 3.7 %, which can be compared to 0.4 % with Mn77Fe[SD], both results have been obtained with a similar solids circulation rate. Although no other results were found with other materials in previous experiments where the ϕ value was in agreement with that shown in Table 5, there is clearly a relevant improvement in combustion efficiency using the Mn77Fe[SD] material when compared to ilmenite, Fe-ESF, and Fe-ore.

3.4. Characterization of the particles used in continuous tests

The Mn77Fe[SD] particles were subjected to physical and chemical characterization before and after their use in continuous CLC tests. Table 6 shows the main features of the MnFe-based particles both fresh and after the CLC combustion tests with gases and coal.

Oxygen transport capacity was maintained after combustion tests in both facilities. This suggests an adequate redox exploitation between the spinel, $(Mn_{0.77}Fe_{0.23})_3O_4$, and the mangano-wüstite, $(Mn_{0.77}Fe_{0.23})O$, in MnFe-based materials for CLC with gaseous and solid fuels. The oxygen uncoupling property of the Mn77Fe[SD] material, which was lost during the calcination procedure, was not recovered during testing in CLC units. With regard to reactivity during reduction of $(Mn_{0.77}Fe_{0.23})_3O_4$, the rate index with H_2, CO, and CH_4 was unchanged after tests burning gaseous fuels. However, an increase of the reaction rate with H_2 and CO, and a decrease in the reactivity with CH_4 were observed after the use of the particles to burn coal. In addition, reactivity for the oxidation reaction increased after the combustion tests.

Table 6. Main features of the Mn77Fe[SD] fresh and used particles.

		Fresh	Used in CLC-CSIC-g1	Used in CLC-CSIC-s1
Oxygen transport capacity (wt.%)		6.7	6.7	6.7
Rate index (%/min)	H_2	13.0	13.6	16.3
	CO	3.9	3.8	5.0
	CH_4	9.6	9.5	4.7
	O_2	7.4	9.5	10.2
Relative permeability (-)	AR[(1)]	2.5	1.9	2.3
	FR[(2)]	-	1.7	2.0
Crushing strength (N)		1.7	1.4	1.0
AJI (%)		0.5	0.5	1.6

[(1)] Corresponding to oxidized state particles.
[(2)] Corresponding to reduced state particles.

The magnetic behavior of the particles was maintained throughout the combustion period. Use can be made of this property to facilitate separation of the oxygen carrier from the ash particles. This gives an added value to the Mn77Fe[SD] material, which would solve the problem of material losses in the ash purge stream.

During the combustion of gaseous fuels, crushing strength decreased from 1.7 N to 1.4 N, which is still a suitable value for an oxygen carrier material [62]. In this sense, it is remarkable that AJI was maintained at a low value of 0.5 %. In addition, the attrition rate was calculated during the combustion of fuel gases in the ICB-CSIC-g1 unit. Elutriated fines particles (d_p < 45 μm) were collected in the filters at a rate of 0.0163 %/h, corresponding to a particle lifetime of 6150 h. This corroborates the good mechanical stability shown by this material during the 10 h of gaseous fuels combustion. However, crushing strength was reduced to a value of 1.0 N after 10 h of coal combustion, which suggests a severe softening of the material. In this case, in order to determine AJI, a previous magnetic separation stage was performed to separate the oxygen carrier particles from the ashes. Consequently, only the oxygen carrier particles were exposed to AJI testing. The AJI value was maintained at the remarkably low value of 1.6 %, lower than the 5-10 % suggested as the upper limit for an oxygen carrier material [62].

Therefore, particle reactivity and mechanical strength was observed to evolve in different way during the combustion of either gaseous fuels or coal. On evaluation of the operating conditions set for these tests, the different oxygen carrier to fuel ratio used is worthy of note. It has recently been suggested that a low oxygen carrier to fuel ratio, which is related to high variation in oxygen carrier conversion during redox cycles in a CLC unit, damages the mechanical integrity of the particles [42]. This is in agreement with the decrease in the mechanical strength of the particles in the experiments with coal, where the oxygen carrier to fuel ratio was ϕ = 1-1.5. In these tests, a high variation of solids conversion in every redox cycle would imply higher chemical stress on the particles, which would decrease the attrition resistance of the material. Despite this, the low AJI value of 1.6 % after coal

combustion in the CLC rig should be highlighted. On the contrary, a high ϕ value during the combustion of gaseous fuels (ϕ = 4.2-9) caused low chemical stress on the particles, and the mechanical integrity of the particles was preserved. Thus, a high oxygen carrier to fuel ratio is advised in order to extend particle lifetime.

Nevertheless, further work must be carried out in order to confirm the results obtained in this work. More combustion time in the CLC units is required in order to demonstrate the reliability of this material before its use in a scale-up of the CLC process. Moreover, the interaction of coal ash with the oxygen carrier material should be evaluated during long-duration testing.

4. Conclusions

Further to the study of an MnFe-based material found in a previous work, an industrial production method, spray drying, was used to manufacture $(Mn_{0.77}Fe_{0.23})_2O_3$ particles. The spray-dried particles required a calcination at 1350 ºC in order to obtain particles with adequate mechanical properties. The solid was almost completely composed of spinel phases, $(Mn_xFe_{1-x})_3O_4$. This led to the loss of the oxygen uncoupling capability of the material due to the slow regeneration of the bixbyite, $(Mn_{0.77}Fe_{0.23})_2O_3$. Nevertheless, high reactivity with gases (i.e., H_2, CO, CH_4 and O_2) and high oxygen transport capacity were achieved during redox cycles between spinel, $(Mn_{0.77}Fe_{0.23})_3O_4$, and mangano-wüstite, $(Mn_{0.77}Fe_{0.23})O$.

The MnFe-based oxygen carrier showed complete fuel conversion to CO_2 and H_2O during the combustion of syngas at fuel reactor temperatures above 930 ºC. However, the maximum combustion efficiency of 78 % at 966 ºC was achieved during the CH_4

combustion. A fuel reactor temperature higher than 1000 ºC is advisable in order to achieve full CH_4 combustion.

During the combustion of different types of coals in *i*G-CLC mode, CO_2 capture rates of 55, 74, and 94% and oxygen demand values of 0.3, 4.4, and 1.5% were achieved for anthracite, bituminous coal, and lignite, respectively. These values represent a relevant improvement in comparison with others low-cost Fe-based oxygen carriers such as ilmenite, Fe-ESF, and Fe-ore. Furthermore, magnetic behavior was shown by the MnFe-based particles, and maintained after the combustion tests. This property gives the MnFe-based material added value because it can be easily separated from ash.

The mechanical integrity of the particles was greatly influenced by the operating conditions used when burning either gaseous fuels or coal. It is believed that the low oxygen carrier to fuel ratio used during coal combustion promoted chemical stress in the particles. Nevertheless, the used particles still demonstrated good behavior in the attrition test. In addition, a high particle lifetime of 6150 h was estimated from the attrition rate observed in the CLC facility when burning gaseous fuels.

In summary, the MnFe-based oxygen carrier in the spinel form can be proposed as a good candidate to be used in *i*G-CLC with coal by taking advantage of its good qualities, namely high reactivity and oxygen transport capacity, as well as magnetic properties.

Acknowledgements

This work was partially supported by the Spanish Ministry for Economy, Industry and Competitiveness (MINECO Projects: ENE2014-56857-R and ENE2016-77982-R projects), by the European Regional Development Fund (ERDF) and by the Spanish National

Research Council (CSIC) via the 2015-80E100 and 2017-80E035 projects. The authors also thank Ing. Konrad Holscher from "Mina Invierno" (Chile) for providing the subbituminous coal used in this work.

Nomenclature

d_p	particle diameter
$(F_i)_{out\,j}$	total molar flow gas of each compound i (i = CO_2, CO, H_2 or CH_4) in the exit stream of each reactor (j = fuel or air reactors) (mol/s)
$F_{O,\,fuel}$	stoichiometric molar flow of atomic oxygen needed to oxidize fully the fuel fed to CO_2 and H_2O (mol/s)
K_m	*relative permeavility (-)*
m	instantaneous mass of the oxygen carrier (kg)
m_{bix}	mass of the sample assuming full oxidized to bixbyite (kg)
m_o^i	mass of oxidized sample between bixbyite and spinel (i = *ou*) or between spinel and mangano-wüstite (i = *g*) (kg).
m_r^i	mass of reduced sample between bixbyite and spinel (i = *ou*) or between spinel and mangano-wüstite (i = *g*) (kg).
$\dot{m}_{OC}$	solids circulation flow rate (kg/h)
m_{OC}^*	specific solids inventory in the fuel reactor (kg/MW_{th})
P_{ref}	reference partial pressure of reacting gas (atm)
P_{TGA}	partial pressure of the gaseous fuel used in the TGA (atm)
R_{OC}^{ou}	oxygen transport capacity by the oxygen uncoupling reaction between bixbyite and spinel (kg oxygen per kg oxygen carrier)
R_{OC}^{g}	oxygen transport capacity by the solid-fuel gas reaction between spinel and mangano-wüstite (kg oxygen per kg oxygen carrier)
R_{OC}^{t}	total oxygen transport capacity of the oxygen carrier between bixbyite and mangano-wüstite (kg oxygen per kg oxygen carrier)
T_{FR}	fuel reactor temperature (ºC)

Greek symbols

ϕ	oxygen carrier-to-fuel ratio
η_{CC}	CO_2 capture efficiency
η_{comb}	combustion efficiency in the fuel reactor
$\tau_{\square c}$	mean residence time of solids in the fuel reactor (s)
Ω_{SF}	oxygen demand of the coal (kg oxygen per kg solid fuel)
Ω_T	total oxygen demand

Acronyms

AJI	Air Jet Index
ANT	Anthracite

BIT	Bituminous
CCHP	Combining Cooling, Heating and Power Production
CLC	Chemical Looping Combustion
CLOU	Chemical Looping with Oxygen Uncoupling
IGCC	Integrated Gasification Combined Cycle
*i*G-CLC	*in-situ* Gasification Chemical Looping Combustion
*e*G-CLC	*ex-situ* Gasification Chemical Looping Combustion
JCPDS	Join Committee on powder Diffraction Standards
NDIR	Non-Dispersive Infrared
LIG	Lignite
SUB	Subbituminous
TGA	Thermogravimetric Analyzer
LHV	Lower Heating Value (kJ/kg coal)
VITO	Flemish Institute for Technological Research
XRD	X-Ray Diffraction

References

[1] International Energy Agency (IEA). CO_2 Emissions from Fuel Combustion. Highlight 2014. Paris, France.

[2] Zhang Z., Cai J., Chen F., Li H., Zhang W., Qi W. Progress in enhancement of CO_2 absorption by nanofluids: A mini review of mechanisms and current status. Renewable Energy 2018;118:527-35.

[3] Zhang Z. Comparisons of various absorbent effects on carbon dioxide capture in membrane gas absorption (MGA) process. J. Nat. Gas Sci. Eng. 2016;31:589-95.

[4] Abanades J.C., Arias B., Lyngfelt A., Mattisson T., Wiley D.E., Li H., Ho M.T., Mangano E., Brandani S. Emerging CO_2 capture systems. Int. J. Greenhouse Gas Control 2015;40:126-66.

[5] Adanez J., Abad A., García-Labiano F., Gayán P., de Diego L.F. Progress in Chemical-Looping Combustion and Reforming Technologies. Prog. Energy Combust. Sci. 2012;38:215-82.

[6] Jin H. and Ishida M. A new type of coal gas fueled chemical-looping combustion. Fuel 2004;83:2411-7.

[7] Jiménez A., López I., González C., Rodríguez J., Nieto R. Simulation of an integrated gasification combined cycle with chemical-looping combustion and carbon dioxide sequestration. Energy Convers. Manage. 2015;104:170-9.

[8] Fan J., Hong H., Zhu L., Wang Z., Jin H. Thermodynamic evaluation of chemical looping combustion for combined cooling heating and power production driven by coal. Energy Convers. Manage. 2017;135:200-11.

[9] Johansson E., Mattisson T., Lyngfelt A., Thunman H. Combustion of syngas and natural gas in a 300 W chemical-looping combustor. Chem. Eng. Res. Des. 2006;84:819-27.

[10] Dueso C., García-Labiano F., Adánez J., de Diego L.F., Gayán P., Abad A. Syngas combustion in a chemical-looping combustion system using an impregnated Ni-based oxygen carrier. Fuel 2009;88:2357-64.

[11] Abad A., Mattisson T., Lyngfelt A., Rydén M. Chemical-Looping Combustion in a 300 W continuously operating reactor system using a manganese-based oxygen carrier. Fuel 2006;85:1174-85.

[12] Abad A., Mattisson T., Lyngfelt A., Johansson M. The use of iron oxide as oxygen carrier in a chemical-looping reactor. Fuel 2007;86:1021-35.

[13] Forero C.R., Gayán P., de Diego L.F., Abad A., García-Labiano F., Adánez J. Syngas combustion in a 500 W_{th} Chemical-Looping Combustion system using an impregnated Cu-based oxygen carrier. Fuel Process. Technol. 2009;90:1471-9.

[14] Kolbitsch F., Bolhàs-Nordenkampf J., Pröll T., Hofbauer H. Operating experience with chemical looping combustion in a 120 kW dual circulating fluidized bed (DCFB) unit. Int. J. Greenhouse Gas Control 2010;4:180-5.

[15] Zheng M., Shen L., Feng X. In situ gasification chemical looping combustion of a coal using the binary oxygen carrier natural anhydrite ore and natural iron ore. Energy Convers. Manage. 2014;83:270-83.

[16] Jerndal E., Mattisson T., Lyngfelt A. Thermal analysis of chemical-looping combustion. Chem. Eng. Res. Des. 2006;84:795-806.

[17] Abad A., García-Labiano F., Adánez J., de Diego L.F., Gayán P., Celaya J. Mapping of the range of operational conditions for Cu-, Fe- and Ni-based oxygen carriers in chemical-looping combustion. Chem. Eng. Sci. 2007;62:533–49.
[18] García-Labiano F., de Diego L.F., Gayán P., Adánez, J., Abad A., Dueso C. Effect of Fuel Gas Composition in Chemical-Looping Combustion with Ni-Based Oxygen Carriers. 1. Fate of Sulfur. Ind. Eng. Chem. Res. 2009;48:2499-508.
[19] de Diego L.F., García-Labiano F., Gayán P., Abad A., Cabello A., Adánez J., Sprachmann G. Performance of Cu- and Fe-based oxygen carrier in a 500 W_{th} CLC unit for sour gas combustion with high H_2S content. Int. J. Greenhouse Gas Control 2014;28:168-79.
[20] Mendiara T., Gayán P., Abad A., García-Labiano F., de Diego L.F., Adánez J. Characterization for disposal of Fe-based oxygen carriers from a CLC unit burning coal. Fuel Process. Technol. 2015;138:750-7.
[21] Adánez J., Abad A., Mendiara T., Gayán P., de Diego L.F., García-Labiano F. Chemical looping combustion of solid fuels. Prog. Energy Combust. Sci. 2018;65;6-66.
[22] Su M., Zhao H., Ma J. Computational fluids dymanics simulation for chemical looping combustion of coal in a dual circulation fluidized bed. Energy Convers. Manage. 2015;105:1-12.
[23] Abad A., Pérez-Vega R., Bueno J.A., Gayán P., García-Labiano F., de Diego L.F., Adánez J. Fluid dynamic characterization of a 50 kW unit for CLC of coal with improved configuration. In proceedings of the 12th International Conference on Fluidized Bed Technology, Krakow, Poland; 2017.
[24] Pérez-Vega R., Abad A., García-Labiano F., Gayán P., de Diego L.F., Adánez J. Coal combustion in a 50 kW_{th} Chemical Looping Combustion unit: Seeking operating conditions to maximize CO_2 capture and combustion efficiency. Int. J. Greenhouse Gas Control 2016;50:80-92.
[25] García-Labiano F., de Diego L.F., Gayán P., Abad A., Adánez J. Fuel reactor modelling in chemical-looping combustion of coal: 2-simulation and optimization. Chem. Eng. Sci. 2013;87:173-82.
[26] Mattisson T., Lyngfelt A., Leion H. Chemical-looping with oxygen uncoupling for combustion of solid fuels. Int. J. Greenhouse Gas Control 2009;3:11-19.
[27] Gayán P., Abad A., de Diego L.F., García-Labiano F., Adánez J. Assessment of technological solutions for improving chemical looping combustion of solid fuels with CO_2 capture. Chem. Eng. J. 2013;233:56-69.
[28] Adánez J., Gayán P., Adánez-Rubio I., Cuadrat A., Mendiara T., Abad A., García-Labiano F., de Diego L.F. Use of Chemical-Looping processes for coal combustion with CO_2 capture. Energy Procedia 2013;37:540-9.
[29] Mendiara T., Adánez-Rubio I., Gayán P., Abad A., de Diego L.F., García-Labiano F., Adánez J. Process Comparison for Biomass Combustion: In Situ Gasification-Chemical Looping Combustion (*i*G-CLC) versus Chemical Looping with Oxygen Uncoupling (CLOU). Energy Technol. 2016;4:1130-6.
[30] Mattisson T. Materials for Chemical-Looping with Oxygen Uncoupling. ISRN Chem. Eng. 2013; ID 526375.

[31] Rydén M., Leion H., Mattisson T., Lyngfelt A. Combined oxides as oxygen-carrier material for chemical-looping with oxygen uncoupling. Appl. Energy 2014;113:1924-32.
[32] Imtiaz Q., Hosseini D., Müller C.R. Review of Oxygen Carriers for Chemical Looping with Oxygen Uncoupling (CLOU): Thermodynamics, Material Development, and Synthesis. Energy Technol. 2013;1:633-47.
[33] Gayán P., Adánez-Rubio I., Abad A., de Diego L.F., García-Labiano F., Adánez J. Development of Cu-based oxygen carriers for Chemical-Looping with Oxygen Uncoupling (CLOU) process. Fuel 2012;96:226-38.
[34] Abad A., Adánez-Rubio I., Gayán P., García-Labiano F., de Diego L.F., Adánez J. Demonstration of chemical-looping with oxygen uncoupling (CLOU) process in a 1.5 kW_{th} continuously operating unit using a Cu-based oxygen-carrier. Int. J. Greenhouse Gas Control 2012;6:189-200.
[35] Adánez-Rubio I., Abad A., Gayán P., de Diego L.F., García-Labiano F., Adánez J. Performance of CLOU process in the combustion of different types of coal with CO_2 capture. Int. J. Greenhouse Gas Control 2013;12:430-40.
[36] Adánez-Rubio I., Abad A., Gayán P., de Diego L.F., García-Labiano F., Adánez J. Biomass combustion with CO_2 capture by chemical looping with oxygen uncoupling (CLOU). Fuel Process. Technol. 2014;124:104-14.
[37] Adánez-Rubio I., Gayán P., Abad A., García-Labiano F., de Diego L.F., Adánez J. Evaluation of a Spray-Dried $CuO/MgAl_2O_4$ as Oxygen Carrier for the Chemical Looping with Oxygen Uncoupling Process. Energy Fuels 2012;26:3069-81.
[38] Pérez-Vega R., Adánez-Rubio I., Gayán P., Izquierdo M.T., Abad A., de Diego L.F., García-Labiano F., Adánez J. Sulphur, nitrogen and mercury emissions from coal combustion with CO_2 capture in chemical looping with oxygen uncoupling (CLOU). Int. J. Greenhouse Gas Control 2016;46:28-38.
[39] Pour N.M., Leion H., Rydén M., Mattisson T. Combined Cu/Mn Oxides as an Oxygen Carrier in Chemical Looping with Oxygen Uncoupling (CLOU). Energy Fuels 2013;27:6031-9.
[40] Hosseini D., Imtiaz Q., Abdala P.M., Yoon S., Kierzkowska A.M., Weidenkaff A., Müller C.R. CuO promoted Mn_2O_3-based materials for solid fuel combustion with inherent CO_2 capture. J. Mater. Chem. A 2015;3:10545-50.
[41] Adánez-Rubio I., Izquierdo M.T., Abad A., Gayán P., de Diego L.F., Adánez J. Spray granulated Cu-Mn oxygen carrier for chemical looping with oxygen uncoupling (CLOU) process. Int. J. Greenhouse Gas Control 2017;65:76-85.
[42] Adánez-Rubio I., Abad A., Gayán P., de Diego L.F., Adánez J. CLOU process performance with a Cu-Mn oxygen carrier for the combustion of different types of coal with CO_2 capture. Fuel 2018;212:605-12.
[43] Pishahang M., Larring Y., Sunding M., Jacobs M., Snijkers F. Performance of Perovskite-Type Oxides as Oxygen-Carrier Materials for Chemical Looping Combustion in the Presence of H_2S. Energy Technol. 2016;4:1305-16.
[44] Frick V., Rydén M., Leion H., Mattisson T., Lyngfelt A. Screening of supported and unsupported Mn-Si oxygen carriers for CLOU (chemical-looping with oxygen uncoupling). Energy 2015;93:544-54.
[45] Shulman A., Cleverstam E., Mattisson T., Lyngfelt A. Manganese/Iron, Manganese/Nickel, and Manganese/Silicon Oxides used in Chemical-Looping With

Oxygen Uncoupling (CLOU) for Combustion of Methane. Energy Fuels 2009;23:5269-75.

[46] Schmitz M., Linderholm C., Lyngfelt A. Chemical Looping Combustion of Sulphurous Solid Fuels using Spray-Dried Calcium Manganate Particles as Oxygen Carrier. Energy Procedia 2014;63:140-52.

[47] Schmitz M., Linderholm C., Lyngfelt A. Chemical-Looping Combustion of Four Different Solid Fuels Using a Manganese-Silicon-Titanium Oxygen Carrier. In proceedings of the 4th International Conference on Chemical Looping Combustion, Nanjing, China; 2016.

[48] Cabello A., Abad A., Gayán P., de Diego L.F., García-Labiano F., Adánez J. Effect of Operating Conditions and H_2S Presence on the Performance of $CaMg_{0.1}Mn_{0.9}O_{3-\delta}$ Perovskite Material in Chemical Looping Combustion (CLC). Energy Fuels 2014;28:1262-74.

[49] Schmitz M. and Linderholm C.J. Performance of calcium manganate as oxygen carrier in chemical looping combustion of biochar in a 10 kW pilot. Appl. Energy 2016;169:729-37.

[50] Azimi G., Leion H., Rydén M., Mattisson T., Lyngfelt A. Investigation of Different Mn-Fe Oxides as Oxygen Carrier for Chemical-Looping with Oxygen Uncoupling (CLOU). Energy Fuels 2013;27:367-77.

[51] Mungse P.B., Saravanan G., Nishibori M., Subrt J.. Labhsetwar N.K. Solvent-free, improved synthesis of pure bixbyite phase of iron and manganese mixed oxides as low-cost, potential oxygen carrier for chemical looping with oxygen uncoupling. Pure Appl. Chem. 2017;89:511-21.

[52] Shafiefarhood A., Stewart A., Li F. Iron-containing mixed-oxide composites as oxygen carriers for Chemical Looping with Oxygen Uncoupling (CLOU). Fuel 2015;139:1-10.

[53] Lambert A., Delquié C., Clémençon I., Comte E., Lefebvre V., Rousseau J., Durand B. Synthesis and characterization of bimetallic Fe/Mn oxides for chemical looping combustion, Energy Procedia 2009;1:375-81.

[54] Larring Y., Braley C., Pishahang M., Andreassen K.A., Bredesen R. Evaluation of a Mixed Fe-Mn Oxide System for Chemical Looping Combustion. Energy Fuels 2015;29:3438-45.

[55] Pérez-Vega R., Abad A., Gayán P., de Diego L.F., García-Labiano F., Adánez J. Development of $(Mn_{0.77}Fe_{0.23})_2O_3$ particles as an oxygen carrier for coal combustion with CO_2 capture via in-situ gasification chemical looping combustion (*i*G-CLC) aided by oxygen uncoupling (CLOU). Fuel Process. Technol. 2017;164:69-79.

[56] Abián M., Abad A., Izquierdo M.T., Gayán P., de Diego L.F., García-Labiano F., Adánez J. Titanium substituted manganese-ferrite as an oxygen carrier with permanent magnetic properties for chemical looping combustion of solid fuel. Fuel 2017;195:38-48.

[57] Wang B., Gao C., Wang W., Zhao H., Zheng C. Sulfur evolution in chemical looping combustion of coal with $MnFe_2O_4$ oxygen carrier. J. Env. Sci. 2014;26:1062-70.

[58] Bhavsar S., Tackett B., Veser G. Evaluation of iron- and manganese-based mono- and mixed-metallic oxygen carriers for chemical looping combustion. Fuel 2014;136:268-79.

[59] Rydén M., Lyngfelt A., Mattisson T. Combined manganese/iron oxides as oxygen carrier for chemical looping combustion with oxygen uncoupling (CLOU) in a circulating fluidized bed reactor system. Energy Procedia 2011;4:341-8.

[60] Rydén M., Källén M., Jing D., Hedayati A., Mattisson T., Lyngfelt A. $(Fe_{1-x}Mn_x)Ti_yO_3$ based oxygen carriers for chemical-looping combustion and chemical-looping with oxygen uncoupling. Energy Procedia 2014;51:85-98.

[61] American Society for Testing and Materials (ASTM). Standard test method of attrition and abrasion of powdered catalysis by air jets. ASTM-D-5757-11. Philadelphia, PA, USA, 2012.

[62] Cabello A., Gayán P., García-Labiano F., de Diego L.F., Abad A., Adánez J. On the attrition evaluation of oxygen carriers in Chemical Looping Combustion. Fuel Process. Technol. 2016;148:188-97.

[63] Mendiara T., Izquierdo M.T., Abad A., Gayán P., García-Labiano F., de Diego L.F., Adánez J. Mercury Release and Speciation in Chemical Looping Combustion of Coal. Energy Fuels 2014;28:2786-94.

[64] Cuadrat A., Abad A., García-Labiano F., Gayán P., de Diego L.F., Adánez J. Relevance of the coal rank on the performance of the in situ gasification chemical-looping combustion. Chem. Eng. J. 2012;195-196:91-102.

[65] Mendiara T., de Diego L.F., García-Labiano F., Gayán P., Abad A., Adánez J. On the use of a highly reactive iron ore in chemical looping combustion with the different coals. Fuel 2014;126:239-49.

[66] Mendiara T., Pérez R., Abad A., de Diego L.F., García-Labiano F., Gayán P., Adánez J. Low-Cost Fe-Based Oxygen Carrier Materials for the *i*G-CLC Process with Coal.1. Ind. Eng. Chem. Res. 2012;51:16216-29.

[67] Crum J.V., Riley B.J., Vienna J.D. Binary Phase Diagram of the Manganese Oxide-Iron Oxide System. J. Am. Ceram. Soc. 2009;92:2378-84.

[68] Bakare P.P., Gupta M.P., Date S.K., Sinha A.P.B. Structural, magnetic and Mössbauer studies on $Mn_xFe_{3-x}O_4$ ($0 \leq x \leq 1$). Proc. Indian Acad. Sci. (Chem. Sci.) 1984;93:1349-59.

[69] Pérez-Vega R. Captura de CO_2 en la combustión de carbón con transportadores sólidos de oxígeno. PhD Thesis, Universidad de Zaragoza, 2016.

[70] Cuadrat A., Abad A., García-Labiano F., Gayán P., de Diego L.F., Adánez J. The use of ilmenite as oxygen-carrier in 500 W_{th} Chemical-Looping Coal Combustion unit. Int. J. Greenhouse Gas Control 2011;5:1630-42.